Morphology of Ethylene−Propylene Copolymer Based Ionomers as Studied by Solid State NMR and Small Angle X-ray Scattering in Relation to Some Mechanical Properties

M. E. L. Wouters,*,† V. M. Litvinov,‡ F. L. Binsbergen,† J. G. P. Goossens,† M. van Duin,‡ and H. G. Dikland‡

Eindhoven Polymer Laboratories, Department of Chemical Engineering, Eindhoven University of Technology, P.O. Box 513, 5600 MB Eindhoven, The Netherlands, and DSM Research, P.O. Box 18, 6160 MD Geleen, The Netherlands

Received March 8, 2002

ABSTRACT: The microphase structure of ionomers based on an amorphous, maleated ethylene−propylene copolymer was investigated by using small-angle X-ray scattering (SAXS) and solid-state NMR experiments. It was shown that in this kind of ionomers grafted maleic anhydride, its salts with Zn^{2+} and a fraction of EPM chain fragments form immobilized, ion-rich aggregates. Three types of EPM chain units with different mobility were detected in the ionomers and in the ionomer precursor, which can be attributed to chain units with low mobility forming aggregates surrounded by an interfacial layer, EPM network chains interconnecting these aggregates, and network imperfections such as dangling ends and chain loops. When the the degree of neutralization is increased, the average dimension of the immobilized aggregate remains almost constant, while the thickness of the interfacial layer with restricted mobility slightly increases. The size of the aggregates in MAn-*g*-EPM ionomers is significantly larger compared to other ionomers, and as a consequence, the number of acid groups within an aggregate is also larger. At 50% neutralization, the number of aggregates suddenly decreases. The changes in some macroscopic properties, such as compression set and tensile properties, are related to the morphology of the ionomers as determined by SAXS and NMR. When the degree of neutralization is increased, the properties of the materials change due to strengthening of the ionic aggregates.

Introduction

Structure and Properties of Ionomers. Ionomers are ion-containing polymers, consisting of polymeric backbones with a relatively small number of monomer units with an ionic functionality either as a pendant group or incorporated in the main chain.[1−4] Mostly, structures with carboxylic, sulfonic, or phosphoric acids are used, which are partially or fully neutralized with (metal) cations. Although many types of ionomers have been developed to date, Surlyn (ethylene−methacrylic acid copolymer based ionomers) and Nafion (perfluorosulfonate ionomers) are the most well-known, commercialized ionomers.

A large number of papers have appeared on the microstructure of ionomers and has shown that as a result of the large difference in polarity the ionic groups tend to form microphase-separated ionic aggregates with sizes on the order of nanometers, dispersed in the hydrophobic polymer. Different ionic aggregates are distinguished, according to the number of ionic groups involved, e.g., multiplets, ionic clusters, or ionic domains. These aggregates are responsible for the unique physicochemical properties of ionomers: since ionomers can behave as thermoreversibly cross-linked or reinforced materials.[1−4]

The thermoreversible nature of the ionic associations makes ionomers with a low glass transition temperature (T_g) interesting candidates for thermoplastic elastomers, i.e., polymers that behave like cross-linked elastomers at service temperature, but that are melt processable at elevated temperatures. An example of such a low T_g, noncrystalline ionomer is metal-neutralized poly(ethylene-*co*-methacrylic acid) (EMAA) with high MAA contents.[5,6] By using high amounts of MAA, the crystallinity is suppressed, but the melt viscosity is also affected. Another example is metal-neutralized sulfonated EPDM, where EPDM is a terpolymer of ethylene, propylene and a diene monomer.[7−10] A substantial improvement in the mechanical properties of EPDM, such as the tensile modulus and the tensile strength, is achieved by the introduction of small amounts of zinc sulfonate groups, obtained by sulfonating the EPDM with acetyl sulfate and subsequent neutralization with zinc acetate. Although at higher temperatures weakening of the ionic interactions occurs, the ionic interactions are too strong and result in very high melt viscosities at conventional processing temperatures. The processability of these zinc-sulfonated EPDMs is enhanced by adding polar plasticizers, which selectively plasticize the ionic aggregates.[11,12] This reduces the melt viscosity substantially, but also deteriorates the mechanical properties.

It has been shown that sulfonated ionomers associate stronger than analogous carboxylated materials.[13] The melt viscosity of the sulfonated ionomers is approximately 2−3 orders of magnitude higher than that of the carboxylated analogues at a given level of functionality and temperature. Therefore, the use of a *carboxylated elastomer* is preferred for practical applications. Additionally, sulfonated elastomers require complete neutralization, because of the corrosivity of the free sulfonic acid groups in partially neutralized ionomers. For

* Corresponding author. Present address: TNO Industrial Technology, Division of Materials Technology, P.O. Box 6235, 5600 HE Eindhoven, The Netherlands. E-mail: m.wouters@ind.tno.nl.
† Eindhoven University of Technology.
‡ DSM Research.

10.1021/ma020358a CCC: $25.00
Published on Web 01/25/2003

carboxylated elastomers *partial neutralization* is allowed and the degree of neutralization can, therefore, be used as an additional variable to control the properties of the ionomer.

In this paper a low T_g ionomer based on an ethylene−propylene copolymer (EPM) will be introduced, which is prepared by modification of EPM with maleic anhydride (MAn). MAn is a suitable monomer to graft onto EPM, because it has a low tendency to homopolymerize, resulting in well-defined monomeric grafts, randomly grafted along the EPM chain.[14] When using a maleated ethylene−propylene copolymer (MAn-*g*-EPM) as ionomer precursor, an ionomer based on a dicarboxylic acid functionality is obtained.

Characterization of Ionomers. As for all polymeric systems, the mechanical properties and the rheology of the MAn-*g*-EPM based ionomers, given the microphase-separated structures, are highly dependent on the morphology. The morphology of ionomers and the structure of the ionic aggregates have been extensively studied, primarily using small-angle X-ray scattering (SAXS). The SAXS profile has a characteristic feature, the so-called *ionic peak* which is usually observed at $q = 0.1-0.4$ Å^{-1} ($q = (4\pi/\lambda) \sin \theta$, where λ is the X-ray wavelength and 2θ is the scattering angle). In some cases, also a strong upturn in scattering intensity is observed near $q = 0$. Several structural models have been proposed to explain both the ionic peak and the upturn. To explain the ionic peak, all models assume ionic aggregates with dimensions of 10−100 Å as the basic scattering entity. The interpretation of the observed *ionic peak* in terms of size, and eventually, the composition of the ionic aggregates depends on the morphological model used to fit the experimental data. Several existing models have been evaluated and the fits for our MAn-*g*-EPM based ionomers have been compared with experimental data.[15,16] The Yarusso and Cooper (Y−C) liquidlike model[17] proved to be the best model for the interpretation of the experimental SAXS-data. The Y−C model comprises of a modified hard-sphere model in which the ionic aggregates have a liquidlike order and a distance of closest approach determined by a surrounding layer of hydrocarbon chains, which have a restricted mobility and are attached to each ionic aggregate. The model was in excellent agreement with the experimentally determined ionic peak of various sulfonated polystyrene systems.[17]

In this study, SAXS measurements of neutralized MAn-*g*-EPM ionomers will be interpreted using the Y−C model. To support the morphological model and to obtain information about (i) the structure of a physical network that is formed due to ion aggregation and (ii) the differences in molecular mobility of the ionic aggregates and the soft matrix solid-state NMR was used.[18] Finally, changes in some mechanical properties of the MAn-*g*-EPM based ionomers will be related to the observed changes in ionomer morphology.

Experimental Section

A. Materials Studied. The following materials were studied: the MAn-*g*-EPM ionomer precursor and six ionomers (zinc salts) with different degrees of neutralization. The ionomer precursor contained 7.33 wt % MAn and was prepared via free radical grafting of MAn onto random ethylene−propylene copolymers (EPM, 45 wt % ethylene, 55 wt % propylene, M_n 11 kg·mol^{-1}) in solution.[15,16] The ionomers were prepared by neutralization of the grafted MAn in solution using zinc acetate to different degrees of neutralization (DN).[15,16] The sample characteristics are described in Table 1.

Table 1. Characteristics of the Ionomers Based on MAn-*g*-EPM (7.33 wt % MAn)

DN (%)	Zn^{2+} content (wt %)	gel content (wt %)
0	0.00	0
10	0.47	3
20	0.99	18
25	1.28	56
50	2.43	78
75	3.62	83
100	4.95	84

The gel content of the ionomers was determined by immersing 2 mm thick compression-molded samples in boiling toluene for 22 h after which the samples were dried to constant weight under a nitrogen atmosphere. The gel content is expressed as the weight percentage of unextracted ionomer.

For SAXS measurements, thin films of the ionomers were pressed between poly(tetrafluoroethylene) sheets at 150 °C in a press. The films were pressed in cardboard sample holders to obtain an uniform sample thickness of 0.33 mm. Water absorption by the ionomers during storage was prevented by placing the freshly prepared samples in sealed sample containers, which contained silica gel.

B. Small-Angle X-ray Scattering (SAXS). 1. Equipment. SAXS data were collected at beamline 8.2 of the Synchrotron Radiation Source (SRS) at the CLRC Daresbury Laboratory, Warrington, U.K. A detailed description of the experimental setup is given elsewhere.[19] The SAXS profiles were collected with a quadrant detector, which was calibrated with silver behenate.[20] A parallel ionization detector was placed in front and after the sample to record the incident and transmitted intensities. The detector was positioned at 1.5 m distance from the sample.[22] All samples were measured for 60 s. The data of the SAXS experiments are presented as the normalized intensity per unit sample volume ($I(q)\{I_e(q)V\}^{-1}$) as a function of q. For this purpose, the obtained experimental data were corrected for background scattering, detector response, and sample thickness (transmittance). The resulting curves were converted to absolute scattering power by comparison with the scattering from a Lupolen standard, measured and corrected by the same procedure as the ionomer samples.[21]

2. Data Analysis. The Y−C model provided the best fit for the MAn-*g*-EPM based ionomers.[16] The ionic aggregates are considered as spherical particles with a high electron dense ionic core with radius R_1 and a shell of hydrocarbons with a restricted mobility with radius R_{CA}. These particles are arranged in a liquidlike degree of order with a closest approach distance between two aggregates of $2R_{CA}$. The model, given by eq 1 and illustrated in Figure 1, has four adaptable fit parameters, i.e., R_1, R_{CA}, V_p and ρ. By fitting the Y−C model to the measured SAXS data, insight in the effects of the various experimental variables on the dimensions (R_1 and R_{CA}) of the scattering particles was obtained. The number of scattering particles can be deduced from the average volume per scattering particle (V_p). The number of scattering particles in the sample volume is equal to V_p^{-1}. Assuming that all grafted MAn units are phase separated from the EPM matrix, which is plausible because of the differences in polarity, the value of the electron density difference between the scattering particle and the EPM matrix (ρ) can provide information about the composition of the scattering particle.

$$\frac{I(q)}{I_e(q)V} = \frac{1}{V_p} V_1^2 \rho^2 \Phi^2(qR_1) \frac{1}{1 + \frac{8V_{CA}}{V_p} \epsilon \Phi(2qR_{CA})} \qquad (1)$$

Statistical Analysis System software (SAS−Institute Inc., Cary, NC) was used to fit the model to the experimental data. The best-fit values of the four model parameters and the corresponding errors were found by a nonlinear least-squares fitting procedure. Table 2 gives an example of the results of a

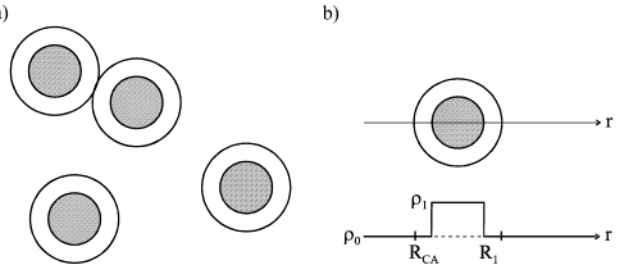

Figure 1. (a) Modified hard sphere model of Yarusso and Cooper.[17] (b) Corresponding electron density profile.

Table 2. Statistical Parameters of the Nonlinear Least-Squares Fitting of SAXS Data for a Zinc Ionomer Based on MAn-*g*-EPM (DN = 20%)

			asymptotic 95% confidence interval	
	estimate	asymptotic std error	lower	upper
R_1 (Å)	22.19	0.13	21.94	22.44
R_{CA} (Å)	44.79	0.09	44.61	44.97
V_p (Å^3)	5.93×10^5	5.9×10^3	5.8×10^5	6.1×10^5
ρ (e·Å^{-3})	0.100	0.001	0.097	0.103

Table 3. Parameter Correlation Matrix

	R_1	R_{CA}	V_p	ρ
R_1	1	−0.44	−0.05	−0.89
R_{CA}	−0.44	1	0.28	0.42
V_p	−0.05	0.28	1	0.46
ρ	−0.89	0.42	0.46	1

zinc ionomers with a DN = 20%. It can be seen that the ionic core has a radius R_1 of about 22 Å and that the radius of closest approach (R_{CA}) is approximately 44 Å. The Newton−Gauss method was used because of its numerical stability and fast convergence.

Besides the best-fit parameter set, the correlation matrix (Table 3) is given, from which information is obtained about the degree of correlation between the parameters. If the parameters are strongly correlated (correlation coefficient is larger than 0.98), problems may arise in finding an unique set of parameters. As can be seen in the parameter correlation matrix, all four parameters are more or less independent for the materials studied and are independent of the sample-to-detector distance.[22] Therefore, the fitting procedure results in an unique set of best-fit values.

C. Solid State NMR. 1. Equipment. The NMR experiments were performed on a Bruker Minispec NMS-120 spectrometer at ^{1}H resonance frequency of 20 MHz. The spectrometer was equipped with a BVT-3000 variable temperature unit. Dry nitrogen was used for cooling or heating the samples.

2. Sample Preparation. NMR experiments were performed on samples as such and on samples in swollen state. Swelling was obtained by addition of a certain amount of deuterated toluene (toluene-d_8, 99.5 at. % of deuterons, Merck). When the solvent was added, the NMR tube was tightly closed with a Teflon cylinder and the sample was stored for 1 day at room temperature before measuring.

3. Pulse Sequences. The spin−lattice relaxation time (T_1) was measured by the inversion−recovery pulse sequence.[23] Solid-echo pulses were used for the signal detection: $180°_x - \tau_1 - 90°_x - \tau - 90°_y - \tau -$ (acquisition). The point in time after the first $90°_x$ pulse $t = 2\tau - t_{90}/2$ was taken as zero, where $t_{90}/2$ is the half time of the 90° pulse. Two different pulse sequences were used to measure the decay of the transverse (spin−spin) relaxation (T_2 relaxation decay) from both the (semi-) rigid and the mobile fractions of the samples. The solid-echo pulse sequence (SEPS),[23] $90°_x - \tau - 90°_y - \tau -$ (acquisition), with pulse spacing $\tau = 10$ μs, was used to record the fast free-induction-decay (FID) from the (semi-)-rigid fraction of the samples. The decays are acquired starting from an echo maximum at $t = 2\tau - t_{90}/2$ after the first pulse. The SEPS does not eliminate the effect of inhomogeneity of the permanent magnetic field H_o of the spectrometer and its inhomogeneity within a sample volume, which arises from inhomogeneous magnetic susceptibility of heterogeneous samples. For this reason, the SEPS cannot be used for accurate measurements of T_2 decays with a decay time longer than about 100−500 μs.

The Hahn−echo pulse sequence (HEPS),[23] $90°_x - \tau' - 180°_x - \tau' -$ (acquisition), was used to record the slow component of the transverse relaxation for the mobile fraction of the samples. The second pulse in the HEPS inverts the nuclear spins of the mobile molecules and an echo signal is formed with a maximum at time $t = 2\tau' - t_{180}/2$ after the first pulse, where $t_{180}/2$ is the half time of the 180° pulse. Through variation of the pulse spacing in the HEPS (τ'), the amplitude of the transverse magnetization is measured as a function of time t. The HEPS allows the elimination of the magnetic field inhomogeneity and of the chemical shift inhomogeneities, and thus, the T_2 relaxation time for mobile materials can be measured accurately.

4. Spin-Diffusion Experiment. A modified Goldman−Shen spin-diffusion experiment was performed according to the method described in the literature.[24,25] Solid-echo pulses with $t_{se} = 10$ μs were used both in the preparation and the detection phases: $90°_x - t_{se} - 90°_y - (t_{se} + t_r) - 90°_{-x} - t_m - 90°_x - t_{se} - 90°_y -$ {acquisition: $A[f(\tau)]$}. A delay time t_r of 100 μs between the maximum of the first solid-echo and $90°_{-x}$ pulse was used to selectively turn the magnetization of the immobilized phase back to the equilibrium. The spin-diffusion experiment was performed twice for each mixing time, t_m, with a 180° phase shift of the first pulse in the second experiment. The FID from the second experiment was subtracted from the FID obtained in the first experiment. The method largely eliminates the T_1 effect from the recovery of the magnetization due to the spin-diffusion.[24] FIDs recorded at different mixing times were analyzed with a least squares software program developed at DSM Research. The program is not only capable of fitting a single FID but can also be used to obtain a best fit of an array of FIDs measured at different mixing times (global fit). The global fit adjusts one T_2 value for each relaxation component of FID in the array. It was found by a separate fit of FIDs that T_2 values were not affected by the mixing time within the accuracy of the measurement. The important improvement of the global fit, as compared with a separate fit of each FID, is the high reliability of the "best fit" values of the relative fractions of the relaxation components.

5. Data Analysis. The characteristic relaxation times, which determine the different slopes in the magnetization decay curves, were obtained by performing a least-squares fit on the data. The T_2 relaxation decay was fitted with a combination of two exponential functions for the Hahn−echo experiments and a combination of a Gaussian and an exponential function for the solid−echo experiments.

D. Mechanical Properties. Tensile tests were performed on a Zwick 1474 tensile tester in a conditioned laboratory at a temperature of 23 °C. Because of the limited amount of ionomer available, the shape of the dumbbell specimens was smaller than described by the ASTM norm. The width and the length of the section of the samples between the clamps were approximately 5 and 20 mm, respectively. The dumbbells were cut from compression-molded sheets with a thickness of approximately 2 mm. The stress was measured as a function of the elongation at a constant elongation speed of 500 mm·min^{-1}. From the stress−strain curve, the tensile strength (TS), the elongation at break (EB), and the stresses at 50% and 100% strain were determined according to ASTM D 412-92. A preload of 0.1 N was applied to set zero length and stress.

For compression set (CS) determination, cylindrical test pieces were compressed between two parallel plates during 22 h at 23 °C (CS_{23}) or at 70 °C (CS_{70}) with a linear deformation of 25%. The compression set (or permanent set) was determined after a relaxation time without deformation of 30 min at ambient temperature according to ASTM D 395, method B.

Table 4. Best Fit Parameters of the Yarusso−Cooper Model and Calculated Characteristic Parameters for Zinc Ionomers Based on MAn-*g*-EPM with a Variation in Degree of Neutralization (7.33 wt % MAn, $\chi = 1.50$ eq·kg^{-1}, $V_{MAn} = 0.043$)

DN (%)	q_{peak} (Å^{-1})	R_1 (Å)	R_{CA} (Å)	V_p (Å^3)	ρ (e$^-$·Å^{-3})	$R_{CA} - R_1$ (Å)	V_1 (Å^3)	V_p^{-1} (Å^{-3})	V_1/V_p	$V_{MAn}/(V_1/V_p)$	Ξ
0	0.061	23.96	46.04	6.18×10^5	0.063	22.08	5.76×10^4	1.62×10^{-6}	0.093	0.46	243
10	0.061	22.64	45.76	6.12×10^5	0.087	23.12	4.86×10^4	1.63×10^{-6}	0.079	0.54	240
20	0.061	21.75	44.94	6.03×10^5	0.106	23.19	4.31×10^4	1.66×10^{-6}	0.071	0.60	237
25	0.061	21.63	45.77	6.71×10^5	0.130	24.14	4.24×10^4	1.49×10^{-6}	0.063	0.68	263
50	0.053	24.78	52.06	1.32×10^6	0.162	27.28	6.37×10^4	7.58×10^{-7}	0.048	0.89	518
75	0.052	25.94	54.04	1.31×10^6	0.184	28.10	7.31×10^4	7.63×10^{-7}	0.056	0.77	514
100	0.052	25.30	53.41	1.06×10^6	0.187	28.11	6.78×10^4	9.43×10^{-7}	0.064	0.67	416

The hardness of the materials was determined according to ASTM D 2240−91 and is expressed in Shore A units.

Results

1. Small Angle X-ray Scattering. The SAXS data obtained from zinc ionomers of MAn-*g*-EPM with degrees of neutralization (DN) between 0% and 100% are shown in Figure 2. The observed peak in the SAXS profile of the ionomer precursor implies that the MAn-*g*-EPM precursor already contains aggregates that differ in electron density from the matrix. The intensity of the scattering peak increases upon increasing DN. Up to 50% neutralization the intensity of the peak increases, while the position of the peak is constant (0.061 Å^{-1}). When DN exceeds 50%, not only does the intensity of the peak increase but also the position of the peak maximum shifts to lower q values, i.e., from 0.061 Å^{-1} for DN = 0% to approximately 0.052 Å^{-1} for DN = 100%.

The SAXS profiles of the series of ionomers were evaluated using the Y−C model. Table 4 presents the best-fit parameters of the model, the volume fraction of grafted MAn (V_{MAn}, see eq 2), the thickness of the restricted mobility layer ($R_{CA} - R_1$), the volume fraction of the scattering particle (V_1/V_p) and the number of grafted MAn units per scattering particle (Ξ, see eq 3).

V_{MAn} calculated using the MAn content (DG = 7.33 wt %) and the average density of EPM (855 kg·m^{-3}) and MAn (1500 kg·m^{-3}):

$$V_{MAn} = \frac{(DG/1500)}{\{(100 - DG)/855\} + (DG/1500)} \qquad (2)$$

Ξ was calculated using the acid content (χ), the average density of the MAn-*g*-EPM (875 kg·m^{-3}), the Avogadro number (N_{Av}), and the average sample volume per scattering particle (V_p):

$$\Xi = \frac{1}{2}\chi(875 \times 10^{-30})\, N_{Av} V_p \qquad (3)$$

The acid content (χ) is the number of moles of carboxyl groups per kilogram of MAn-*g*-EPM and is equal to 1.50 equiv·kg^{-1}.

When the DN is increased, the SAXS peak position increases. In the region of 0−50% neutralization, R_1 decreases slightly (approximately 2 Å), which may be explained by the tightening of the aggregate as a result of the formation of ionic bonds. The sudden shift of the peak at DN = 50% is reflected by the increase of R_1, which in turn may be explained by the change in the coordination mechanism of the grafted MAn with the zinc cation. Upon neutralization to 50%, only one of the two available MAn-derived acid groups is involved in the coordination with the counterion. Only for neutralization levels beyond 50% the second carboxylic acid group is involved in the coordination of the cation. Because of the steric arrangement and the aggregation of the acid groups, Ξ increases when DN exceeds 50%.

When the DN is increased, V_{MAn} increases. It is anticipated that the polarity of the aggregate increases and, as a consequence, the packing of the aggregate will be denser. The electron density difference between the aggregates and the matrix originates from the grafted MAn and the cations present. The electron density of the scattering aggregate is calculated using V_{MAn}, V_p, and V_1 and the electron densities of MAn, its salt and EPM ($\rho_{MAn-salt}$ and ρ_{EPM} respectively). Equation 4 can be used to calculate the electron density difference between the aggregate and the matrix:

$$\rho_{calculated} = \left(\frac{\{V_p V_{MAn} \rho_{MAn-salt}\} + \{(V_1 - (V_p V_{MAn}))\rho_{EPM}\}}{V_1}\right) - \rho_{EPM} \qquad (4)$$

$$\rho_{MAn-salt} = \frac{(100 - DN)\rho_{MAn} + (DN)\rho_{ZnAc_2}}{100} \qquad (5)$$

With $\rho_{EPM} = 0.293$ e$^-$·Å^{-3}, $\rho_{MAn} = 0.468$ e$^-$·Å^{-3}, and $\rho_{ZnAc2} = 0.531$ e$^-$·Å^{-3}.

The comparison of $\rho_{calculated}$ and the fitted value for ρ from the Y−C model (ρ_{model}) as a function of DN is presented in Figure 3. The discrepancy between the calculated and the fitted values of ρ at low DN may be due to the use of the electron density of crystalline zinc acetate dihydrate in the calculations, while the ionic packing in the ionic aggregates at low DN will be less dense.

It can be concluded that the ionic aggregates contain, besides the polar groups, EPM chain fragments. In Figure 4, a schematic representation of such an aggregate in MAn-*g*-EPM based ionomers is given. This schematic representation suggests that the electron density profile of the aggregate is not constant within the spherical aggregate, while in the Y−C model a

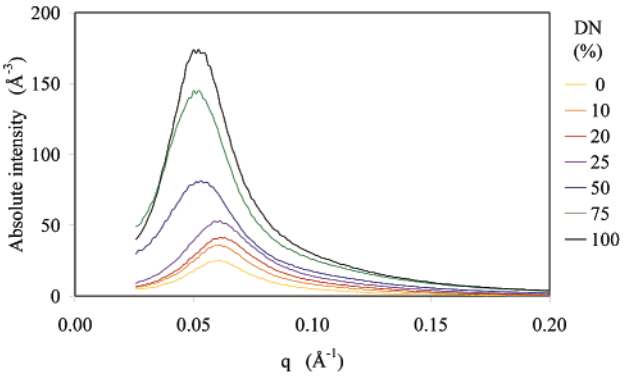

Figure 2. SAXS profiles for zinc ionomers based on MAn-*g*-EPM (7.33 wt % MAn) with various degrees of neutralization (DN).

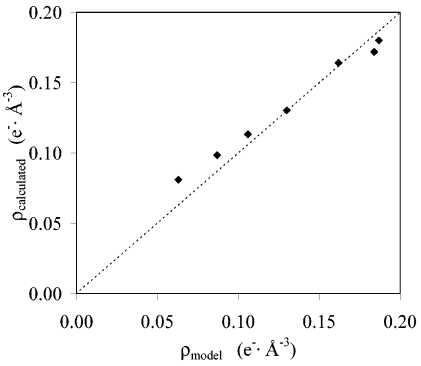

Figure 3. Comparison of the estimated electron density difference using the Yarusso−Cooper model (ρ_{model}) and the calculated electron density difference ($\rho_{calculated}$).

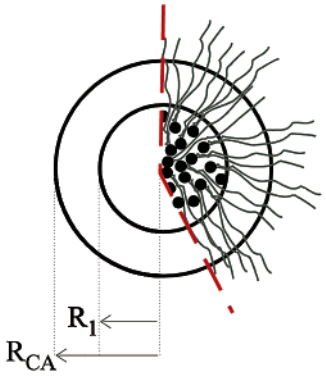

Figure 4. Schematic representation of an aggregate in MAn-*g*-EPM based ionomers and ionomer precursors; the black spots represent grafted MAn units (neutralized and un-neutralized).

constant electron density in the scattering particle is assumed. In the case of modification of the electron density profile in the Y−C model by a radius-dependent profile, the scattering profile does not change significantly.[15,16] Therefore, the original concept as proposed by Y−C[17] was used for the evaluation of the SAXS profiles of the MAn-*g*-EPM based ionomers, because interpretation of the results of the fitting is more straightforward.

2. Solid State NMR. 2.1. ^{1}H NMR Spin—Lattice Relaxation Experiments. The T_1 relaxation time was determined as a function of temperature for samples with varying DN. For all samples, T_1 increases from 75 to about 325 ms upon increasing temperature from 40 to 120 °C. A comparison of the temperature dependence of T_1 does not reveal a significant difference between MAn-*g*-EPM and the completely neutralized ionomer. This means that the local segmental mobility of the majority of the EPM chain units is hardly affected by neutralization of the grafted MAn, although the SAXS results have shown that the samples contain (immobilized) aggregates. Since a single exponent describes the T_1 relaxation at all temperatures, the spin-diffusion between immobilized aggregates and the soft matrix is very efficient in the samples. Therefore, it can be suggested that the size of the immobilized aggregates is smaller than 50 nm.[23]

2.2. ^{1}H NMR Spin−Spin Relaxation Experiments. ^{1}H T_2 relaxation measurements are a very sensitive tool to study the dynamics of elastomer chains and motional heterogeneity.[18] The T_2 relaxation decay of EPM ionomers has a complex shape, which is rather similar for all samples. As an example, the decay for one of the samples is shown in Figure 5.

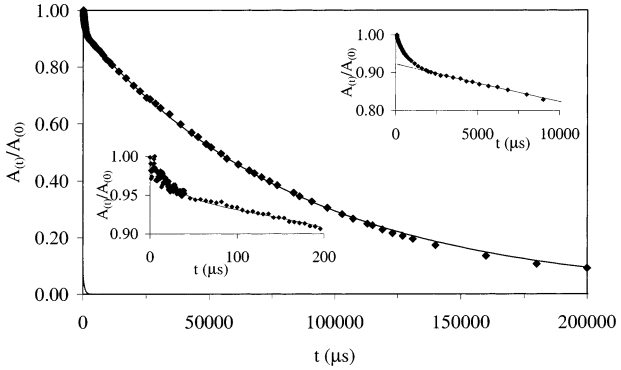

Figure 5. Decay of the transverse ^{1}H magnetization at 90 °C as measured by the Hahn−echo pulse sequence. The inset on the right represents the initial part of the decay as measured by the Hahn−echo pulse sequence. The inset on the left represents the initial part of the T_2 decay as measured by the solid−echo pulse sequence. Solid lines represent the result of a least-squares fit of the decay.

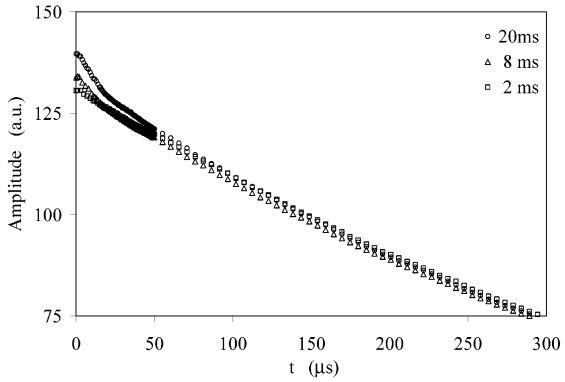

Figure 6. Free induction decay at mixing time of 2, 8, and 20 ms in the spin-diffusion experiment for 100% neutralized zinc ionomer of MAn-*g*-EPM. Only the initial part of the decays is shown in the figure.

The T_2 relaxation for the samples can be described by three components with a short (T_2^s) decay time as measured by the SEPS, and an intermediate (T_2^{in}) and a long (T_2^l) decay time that are determined by the HEPS experiments. The T_2^s values of MAn-*g*-EPM and the ionomer samples are similar and are equal to 0.015−0.018 ms. These values of T_2 are typical for rigid materials and molecules experiencing strongly hindered local molecular mobility.[23,26] Therefore, this relaxation is assigned to *low mobile EPM chain units and grafted MAn in aggregates with a core that contains grafted MAn chain units and its salts with* Zn^{2+}.

The spin diffusion experiments prove the assignment of the T_2^s relaxation to the immobilized chain fragments in the aggregates. Upon variation of the mixing time, the T_2^s relaxation component vanishes at short mixing time and gradually recovers to the equilibrium value with increasing mixing time (Figure 6).

This type of behavior provides strong evidence for the presence of immobilized aggregates in the soft matrix. The recovery of the longitudinal magnetization of immobilized material, $M_r(t_m)/M_r^{eq}$, is shown in Figure 7 for MAn-*g*-EPM with DN of 10% and 100%.

The recovery rate for both samples is about the same, which suggests a similar size of the immobilized aggregates.

The assignment of T_2^{in} and T_2^l is less unambiguous than that of T_2^s. A quantitative analysis of the decay shape for viscoelastic materials or phases is not always

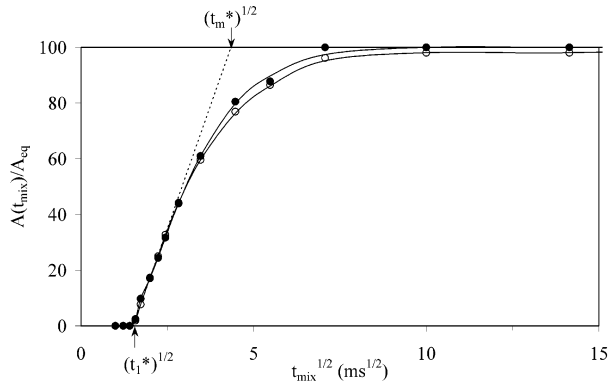

Figure 7. Results of the spin-diffusion experiment which show the recovery of the magnetization of the immobilized material to its equilibrium value. The recovery factor $A(t_{mix})/A_{eq}$ for DN 10% and 100% is shown with solid and open circles, respectively.

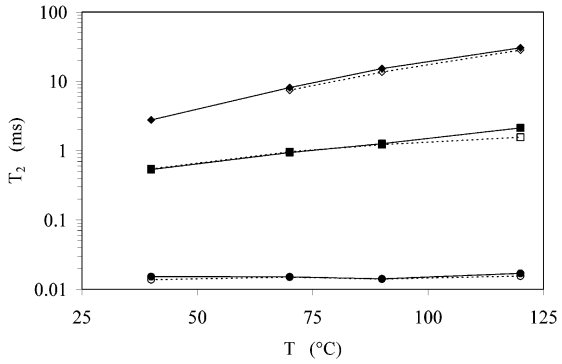

Figure 8. Temperature dependence of T_2 relaxation times (T_2^{index}) for MAn-*g*-EPM and the corresponding 100% neutralized zinc ionomer: (●) T_2^s precursor; (■) T_2^{in} precursor; (♦) T_2^l precursor; (○) T_2^s ionomer; (□) T_2^{in} ionomer; (◊) T_2^l ionomer.

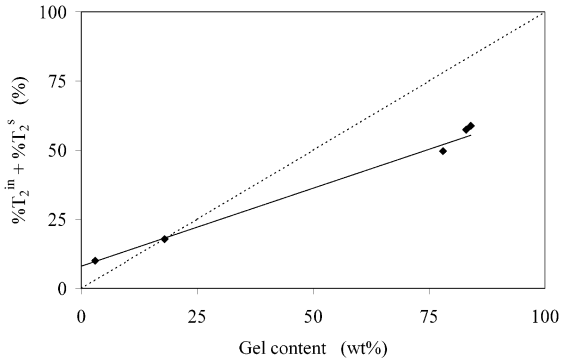

Figure 9. Content of network material as determined by NMR as a function of the gel content as determined by extraction in toluene.

straightforward due to the complex origin of the relaxation itself[27] and the apparent heterogeneity of the ionomer samples studied. Above 360 K, T_2^{in} is close to 1 ms and is in the range which is typical for EPDM vulcanizates at temperatures well above T_g[28] (Figure 8). This relaxation time shows a moderate increase when the samples are swollen in a good solvent (Figure 10a), which is comparable to the behavior of permanent networks.[28] Tentatively, T_2^{in} is assigned to the relaxation of *EPM network chains that connect neighboring aggregates and/or entangled loops*. The relaxation time T_2^{in} is slightly larger for samples with smaller DN

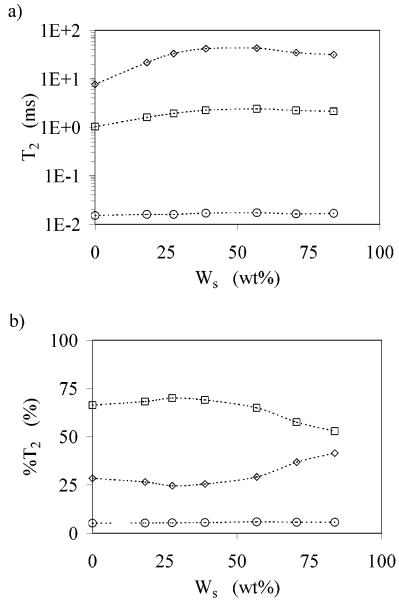

Figure 10. Effect of the percentage of toluene-d_8 on (a) T_2 relaxation times and (b) fractional amplitudes of the relaxation components for a completely neutralized ionomer: (○) T_2^s, $\%T_2^s$; (□) T_2^{in}, $\%T_2^{in}$; (◊) T_2^l, $\%T_2^l$.

(Figure 8). The longer T_2^{in} corresponds to a larger molar mass of network chains,[28] which is related to smaller cluster content, as determined by $\%T_2^s$ (Figure 11). The third relaxation component is characterized by the long decay time T_2^l. The T_2^l value increases continuously with increasing temperature and is much longer than T_2^{in}. Its value is close to the lower limit of T_2 for molten, low-molar-mass polymers and dangling chain-ends.[29−31] This component is assigned to network imperfections such as *polymer chains that are not connected to the aggregates, dangling chains and long chain loops*.

The large difference in the decay time of the different relaxation components indicates that the local motion of EPM chains units adjacent to the ionic core of the aggregate is strongly hindered compared with the chains outside this layer. In reinforced rubbers, the chain units at the rubber−filler interface exhibit the same behavior.[26,32−34]

The relative fraction of the relaxation components, $\%T_2^s$, $\%T_2^{in}$ and $\%T_2^l$, represent the hydrogen fraction of MAn-*g*-EPM immobilized aggregates, network chains and network imperfections, respectively. The total fraction of network chains and aggregates, ($\%T_2^s + \%T_2^{in}$), is plotted against the gel content as determined in toluene in Figure 9. The sum of $\%T_2^s$ and $\%T_2^{in}$ does not differ drastically from the gel content.[35] This gives an additional support for the assignment of the T_2^{in} to the relaxation of network chains. For the sample with DN = 10%, ($\%T_2^s + \%T_2^{in}$) is larger compared to the gel content (see Figure 9). This is possibly caused by the more severe extraction conditions compared to those of the NMR experiments for swollen samples. It has to be noted that the NMR experiments have been performed for swollen samples containing 50 wt % of the solvent, contrary to the extractions, which have been performed with an excess of solvent and at higher temperatures. These more severe extraction conditions result possibly in the destruction of a significant fraction of aggregates. ($\%T_2^s + \%T_2^{in}$) is smaller compared to the gel content for samples which have a DN larger than 10%, which suggests that the gel fraction in these

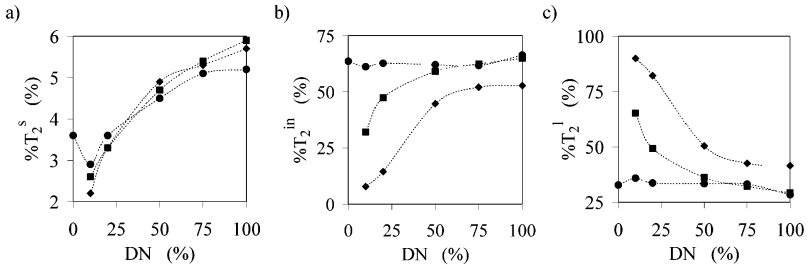

Figure 11. Dependence of the fractional amplitudes of the relaxation components on DN and the amount of toluene-d_8 added (W_s). (a) T_2^s; (b) T_2^{in}; (c) T_2^l; (●) $W_s = 0$ wt %; (■) $W_s = 55$ wt %; (◆) $W_s = 83$ wt %.

samples contain significant fractions of imperfections which contribute to the T_2^l relaxation component.

In conclusion, the relaxation data for the ionomer precursor and the completely neutralized ionomer are rather similar. Since aggregates are present both in the nonneutralized precursor and in the ionomers, both grafted MAn and its corresponding ionic form are incorporated in the aggregates. The hydrogen fraction in the aggregates for the ionomer precursor equals 2.5 at. % and is larger than the hydrogen fraction of grafted MAn in the sample, which equals 1.64 at. %. This implies that the immobilized aggregates are formed by grafted MAn and immobilized EPM chain fragments within the ion-rich aggregate core and adjacent to it. The content of immobilized aggregates gradually increases from approximately 2.5−5.5 at. % of hydrogen with increasing DN (see Figure 11a). It has to be noted that the weight fraction of the aggregates should be approximately 4−6 times larger than $\%T_2^s$ because Zn^{2+} ions do not contribute to $\%T_2^s$ as they are not detected by the ^{1}H NMR relaxation experiment. Furthermore, grafted MAn, which is incorporated in the aggregates, contains approximately 4.7 times less hydrogen per weight unit compared to EPM chains.

2.3. Estimation of the Size of Immobilized Aggregates. The spin-diffusion data in Figure 7 are used for semiquantitative analysis of the aggregate size. The magnetization of the mobile phase is selected with the Goldman−Shen experiment. The flow of the magnetization from the mobile phase (the relaxation source) to the immobilized one (sink) shows an S-like shape, which is typical for materials containing an interface with chain mobility intermediate between that for immobilized and mobile phases.[36,37] The thickness of the interface can be estimated from the intersection of the linear part of the spin-diffusion curve with the time axis, $(t_i^*)^{1/2}$, using the following formula.[37]

$$d_{\text{interface}} = (kD_{\text{interface}}t_i^*)^{1/2} \qquad (6)$$

where the dimensionality parameter k equals $^4/_3$, and the spin-diffusion coefficient of the interface $D_{\text{interface}} = (D_{\text{rigid}} + D_{\text{mobile}})/2$. The k value of $^4/_3$ corresponds to lamellar geometry, which might be also used for spherical rigid aggregates surrounded by semirigid interface shell. It is mentioned that the spin-diffusion coefficient cannot be determined accurately for disordered polymers with complex chemical structures and materials those morphology is not well-defined. A typical value of D_{rigid} of about 0.7 nm^2/ms is used for the estimation of the aggregates size.[36] The spin-diffusion coefficient in the mobile phase, D_{mobile}, could be estimated from the following equation if the longest T_2 relaxation rate in the mobile phase is in the range of $0 < (T_2^{\text{mobile}})^{-1} < 1000$ Hz:[38]

$$D_{\text{mobile}} = (8.2 \times 10^{-6}T_2^{-1.5} + 0.007)\ \text{nm}^2/\text{ms} \qquad (7)$$

Using a T_2^l value of 3 ms, D_{mobile} and $D_{\text{interface}}$ equal 0.007 and 0.35, respectively.

The radius of the immobilized aggregates, d_{rigid}^*, can be estimated using the following equation:[39]

$$d_{\text{rigid}}^* = \frac{r_A\phi_A + r_B\phi_B}{\phi_A\phi_B}\,\frac{\sqrt{D_AD_B}}{r_A\sqrt{D_A} + r_B\sqrt{D_B}}\,\frac{4\epsilon\phi_{\text{dispersed}}}{\sqrt{\pi}}(\sqrt{t_m^*} - \sqrt{t_i^*}) \qquad (8)$$

where $\mathbf{r}_A$ and $\mathbf{r}_B$ are the specific densities of the mobile and rigid phase, ϕ_A and ϕ_B are the volume fractions of the phases, $\phi_{\text{dispersed}}$ is the volume fraction of the dispersed phase, and ϵ is the dimensionality parameter, which equals 3 for spherical shape of the dispersed phase. This equation does not describe rigorously the case of the three-dimensional diffusion for a spherical morphology. It is derived for the lamellar morphology and is a good approximation for a spherical morphology if the radius of the spheres is larger than the thickness of the outer interfacial layer. It is suggested in the calculations below that $r_A \approx r_B$, and $\phi_{\text{dispersed}} \approx \%T_2^s$. Under assumptions above, the radius of immobilized aggregates and the interface thickness is on the order of 1.6 and 1.0 nm, respectively. The estimated aggregates size suffers from a large error because the derivation of eq 8 is based on several assumptions,[36−39] and because the values of D_{rigid}, $D_{\text{interface}}$, and D_{mobile} are approximate ones. Nevertheless, the estimated radius of the immobilized aggregates is comparable to the radius of a dense ionic core (R_1) obtained from the SAXS data, i.e., 1.6 and 2.2 nm, respectively. The radius of the immobilized aggregates surrounded by the interface, which is estimated from the spin-diffusion experiment, is in the same order as the radius of the dense ionic core and a shell of hydrocarbons with a restricted molecular mobility (R_{CA}), as determined from the SAXS data, i.e., 2.6 and 4.5−5.4 nm, respectively. It should be noted that the aggregates size could also depend on the specific technique used for the analysis due to a different in the contrast immobilized and soft phases in the SAXS and spin-diffusion experiments, which can also explain observed differences in the results of both methods.

2.4. Molecular Weight of EPM Network Chains Formed Due To Ionic Interactions. The T_2 value for elastomer networks is quantitatively related to the

number of statistical segments between chemical crosslinks and chain entanglements at temperatures approximately 100−150 °C above T_g.[28,40−42] Assuming Gaussian chain statistics, i.e., the number of rotatable backbone bonds in network chains is larger than 50, the network density can be determined from the plateau T_2 value (T_2^p) since T_2^p is related to the number of statistical segments between network junctions.[28,40,41]

$$T_2^{\,p} = aT_2^{\,rigid}Z \tag{9}$$

Here T_2^p is the observed plateau value at (T_g^{NMR} + 150 °C)[40,41] and $T_2^{rigid} = 10.4 \pm 0.2\ \mu$s, measured for toluene-$d_8$ swollen samples at −133 °C.[28] T_2^{rigid} is related to the strength of the intrachain dipole−dipole interactions in the rigid lattice. The coefficient a in eq 9 is a constant which has a value of approximately 6.2 ± 0.7 for aliphatic chains.[40,41] Z is the number of statistical segments between network junctions and is related to M_c, the weight-average molar mass of the chains between network junctions, by

$$M_c = \frac{ZC_\infty M_u}{n} \tag{10}$$

In this equation M_u represents the average molar mass per two backbone carbon atoms, n is the number of rotatable backbone bonds in an elementary chain unit, and C_∞ is the number of rotatable backbone bonds of the statistical segment. The EPM copolymer used contained 55 wt % propylene and 45 wt % ethylene. The average molar mass per elementary chain unit (M_u) equals 34.35 g·mol^{-1}, and n equals 2. A value of 6.62 for C_∞[43] was used for the estimation of M_c.

Since T_2^{in} is related to the relaxation of the network chains, its value of approximately 0.95 ± 0.05 ms is used for the calculations of the M_c. The molar mass of network chains is then estimated to be approximately 1500−1800 g·mol^{-1}, which agrees well with the average molecular weight between grafted MAn units, which is calculated to be 1520 g·mol^{-1}.

2.5. The Fraction of Network Chains and Network Defects. The analysis of network imperfections in permanent EP(D)M networks is somewhat complicated because of the high physical entanglement density in EP(D)M, which is often comparable to the density of the permanent network junctions. At the time scale of the NMR experiment, which is on the order of milliseconds, the chain entanglements restrict the long spatial scale dynamics of chains in the same way as permanent junctions.[28] It is known that the effect of transient chain entanglements on the chain dynamics decreases as the volume fraction of a solvent in a swollen matrix increases.[27] At relatively high solvent content, the T_2 relaxation of network chains and network defects is different since network chains and defects are disentangled.[28,44] Therefore, the T_2 experiments for swollen matrixes can provide more reliable information on the network heterogeneity and network defects.[34]

Figures 10 and 11 show the change in the relaxation parameters as a function of increasing weight fraction of toluene-d_8 (W_s) in a swollen, completely neutralized MAn-*g*-EPM ionomer. The fraction of immobilized aggregates (%T_2^s) and T_2^s are not affected by the solvent content, which suggests strong ionic interaction within the aggregates. For W_s < 40 wt %, both relaxation times

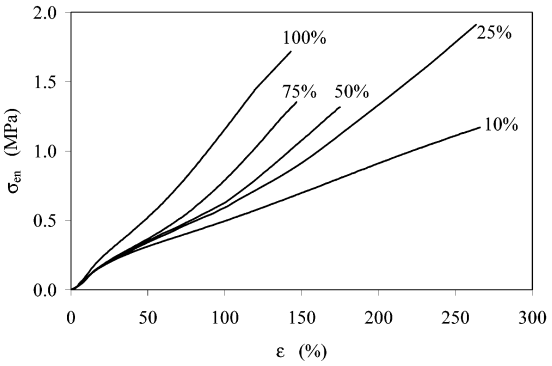

Figure 12. Engineering stress vs strain of zinc ionomers based on MAn-*g*-EPM (7.33 wt % MAn) with a variation in the degree of neutralization (DN = 10−100%).

Table 5. Effect of Degree of Neutralization on Stress−Strain Characteristics of Zinc Ionomers Based on MAn-*g*-EPM (7.33 wt % MAn)

DN (%)	hardness (Shore A)	CS_{23} (%)	CS_{70} (%)	TS (MPa)	EB (%)	σ_{50} (MPa)	σ_{100} (MPa)
0	42	48	100				
10	44	44	92	1.16	265	0.318	0.508
25	45	37	65	1.87	268	0.348	0.609
50	47	26	43	1.24	174	0.352	0.625
75	50	21	35	1.37	146	0.383	0.824
100	52	16	31	1.72	143	0.530	1.166

T_2^{in} and T_2^l increase as the W_s value increases which is mainly caused by the chain disentanglement.[27,28] The fraction of network chains decreases slightly with increasing W_s for W_s > 40 wt %, which suggests that some rearrangement of the network structure due to swelling takes place. The T_2^{in} changes to a smaller extent compared to T_2^l. The fractional amplitude of T_2 relaxation components, as measured in the swollen state at W_s = 55 and 83 wt %, differ significantly at different DN, as can be seen in Figure 11.

The major difference among the swollen samples is observed for the content of the network chains. The network fraction decreases with increasing solvent content for samples with small DN, but the fraction of network chains is not largely affected by the solvent content when DN exceeds 50%. Since the fraction of aggregates and their size, from SAXS, is similar for samples with small and large DN, the model that is presented in the discussion could explain a decrease in the fraction of network chains.

3. Mechanical Properties and Structure. The final goal of this study was to relate the morphological characteristics of the ionomers with the macroscopic properties. Therefore, some mechanical properties of the materials described above were determined, and the results are summarized in Table 5. The tensile data of the ionomers used in the present study will be evaluated for large deformations only. As can be seen in Figure 12, in which the engineering stress is plotted vs strain, the dependence is close to linear at large deformations (neo-Hookean behavior). This implies that the tensile modulus can be related to the strength of the "crosslinks" .

It can also be observed that the slope of the curve at high elongations increases upon increasing DN, suggesting that the strength of the ionic aggregate is insufficient to keep the physical network intact at low DN. For the ionomers tested, it was observed that upon increasing DN the hardness and the stress at interme-

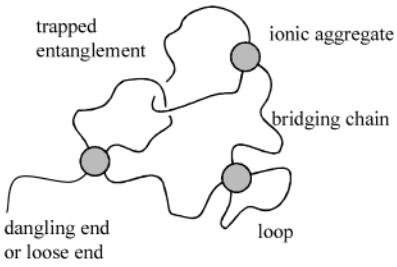

Figure 13. Schematic representation of the ionomer network with (trapped) entanglements, ionic aggregates (cross-links), loops, bridging chains, and dangling ends[50−52]

diate elongation (σ_{xx}) increase and that the compression set (CS) and elongation at break (EB) decrease upon increasing DN. The properties of the ionomeric, cross-linked elastomers show a behavior comparable to the behavior of conventional covalently cross-linked elastomers.

Discussion

In the previous sections, it was shown that grafting of polar MAn groups onto the EPM backbone results in the formation of grafted MAn-rich aggregates, which are phase separated from the apolar EPM matrix. Upon (partial) conversion of the anhydride to the metal carboxylate these aggregates remain and are actually strengthened upon increasing DN. The SAXS characterization of the ionomers, discussed above, suggests that these aggregates are approximately spherical and for the partially neutralized samples consist of metal carboxylates and carboxylic acid groups and for the fully neutralized samples consist mainly of metal carboxylates.

The size of the ionic aggregates is rather large and, concomitantly, a large fraction of grafted MAn units is present in a single aggregate. It is proposed that the grafted MAn groups are anchored fairly solidly in the aggregates. As a result, the aggregates act as multifunctional cross-links for the elastomer chains. The EPM chains between grafted MAn groups either interconnect neighboring aggregates or form loops at the same aggregate. In summary, the EPM chains in ionomers are present as (1) elastically effective chains between ionic cross-links, (2) elastically ineffective loops and dangling ends, (3) possibly entangled loops that give a contribution to elasticity, and (4) soluble EPM chain fragments that do not contain grafted MAn. Since the MAn-*g*-EPM used has a low molecular weight, it is expected and confirmed by NMR T_2 relaxation experiments that the network contains a significant fraction of dangling chain ends. Figure 13 shows a schematic representation of the suggested ionomer network.

When the DN of the MAn-*g*-EPM based ionomers is increased, CS as well as EB decrease, while TS, hardness and gel content increase. This shows a strong resemblance with the effect of increasing cross-link density in covalently cross-linked elastomers. However, when comparing the properties of ionomers with those of conventionally cross-linked elastomers, it has to be kept in mind that these materials differ in the type of network junctions. On one hand, the network density and its topology in the covalently cross-linked materials is not affected by the tensile test. In addition, at a moderate deformation, when chain scission does not occur, it is known that trapped entanglements can provide a large contribution to the properties of covalently cross-linked elastomers.[45] On the other hand, in the case of ionomers, the ionic aggregate, which acts as a multifunctional cross-link junction, may be subject to disruption by the applied stress. Thus, for ionomers, the properties depend not only on the number of aggregates but also on the strength of the aggregates, and therefore, a simple and straightforward correlation between structure and properties is not always possible.[46]

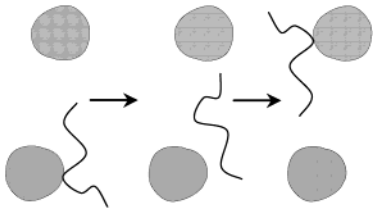

Figure 14. Schematic drawing of "ion hopping" of a segment of a polymer chain bearing a single ionic group.

On the basis of NMR and SAXS results, it was concluded that the aggregates are composed of both the grafted MAn, its salts and even some EPM chain fragments. Relatively weak dipolar interactions and hydrogen bonds are responsible for the cluster formation in the case of the ionomer precursor, while much stronger ionic bonds are formed in the zinc maleate ion aggregates in the ionomers. Thus, the strength of the aggregates increases with increasing DN. The size of the aggregates remains almost the same upon increasing DN, but the restricted mobility layer increases substantially.

Correlating all structural observations with the mechanical properties, the strength of these ionic aggregates seems to be the determining factor for the mechanical properties of the ionomer. The ionic aggregates in the EPM matrix can be connected by entangled loops and bridging chains. The length of chains loops and bridging chains varies in a certain range due to statisctical distribution of EPM chain portions between MAn units and a random distribution of the size and spatial arrangement of the ionic aggregates in the EPM matrix. As long as the ionic aggregates are not disrupted, loops and bridging chains bear the force and contribute to the rubber elasticity. At a certain extension, the polymer chain fragments that form short interlocking loops and short bridging chains will be fully stretched, while full extension will not be reached for longer interlocking loops and longer bridging chains. Upon stretching, one of two events may occur. If the ionic aggregates are highly cohesive and do not rupture, the polymer chains must break. When the aggregates are weakly cohesive, the overloaded chain portions can relax by "ion hopping" and/or pulling the ionic groups out of the aggregates. This mechanism of stress relaxation is visualized in Figure 14 in which a chain fragment at different stages of deformation is shown.[47−49] The ionic aggregates are represented in this figure by beads and the segment of a polymer chain bearing a single ionic group is represented by the curved line. Upon deformation, this particular chain fragment hops from one aggregate to another aggregate resulting in redistribution of the stress.

Conclusions

In this paper, the results of SAXS and solid-state NMR were discussed in order to relate the macroscopic properties of MAn-*g*-EPM based ionomers with underly-

ing morphology. The obtained SAXS data were interpreted using the Y−C model. According to this model the morphology can be described by spherical aggregates of high electron density surrounded by a layer with restricted mobility embedded in a matrix of EPM. According to SAXS and NMR spin-diffusion analysis, the radius of the aggregates is about 1.5−2 nm and the thickness of the interface is about 1−1.5 nm. ^{1}H NMR relaxation experiments also showed that the immobilized aggregates consist not only of grafted MAn and its salts with Zn^{2+} but also of a fraction of adjacent EPM chain units anchored to the aggregates. These aggregates are present in the ionomer precursor materials as well as in the ionomers. The results observed with SAXS also showed a tightening of the aggregate upon increasing DN, which is in agreement with NMR data that suggest that the strengthening of aggregates increases upon increasing DN. The results of the NMR experiments on swollen samples support this conclusion. The estimated mean molar mass of network chains which are formed by ionic bonds and chain entanglements is approximately 1500−1800 g·mol^{-1}. The determination of structure−property relations of ionomers is complex and not straightforward, because of strain-induced rearrangement of the ionic aggregates. Combination of results of the morphological data and the macroscopic properties of the ionomers have let us to suggest that the strength of the ionic aggregates is the determining factor for the mechanical properties of the ionomer.

Acknowledgment. The authors wish to thank DSM Research for financial support. We also thank Prof. T. Michels (Eindhoven University of Technology) for helpful discussions on the modeling of the SAXS results. It is a pleasure to acknowledge Dr. A. Buda, Prof. D. E. Demco, and Prof. B. Blümich for discussions of the NMR spin-diffusion data and providing us with unpublished simulations of the spin-diffusion in materials with extended interfaces. Dr. Günther Grossmann of the CLRC Daresbury Laboratory is acknowledged for his assistance during the SAXS measurements. The silver behenate was a kind gift of Dr. Tom Blanton from Kodak.

References and Notes

(1) *Ionic Polymers*; Holliday, L., Ed.; Applied Science Publishers: London, 1975.
(2) *Ions in Polymers*; Eisenberg, A., Ed.; Advances in Chemistry 187; American Chemical Society: Washington, DC, 1980.
(3) *Ionomers: Characterizations, Theory, and Applications*; Schlick, S., Ed.; CRC Press Inc.: Boca Raton, FL, 1996.
(4) *Ionomers: Synthesis, Structure, Properties and Applications*; Tant, M. R.; Mauritz, K. A., Wilkes, G. L., Eds.; Chapman & Hall: London, 1997.
(5) Kutsumizu, S.; Tagawa, H.; Muroga, Y.; Yano, S. *Macromolecules* **2000,** *33*, 3818.
(6) Kutsumizu, S.; Tadana, K.; Matsuda, Y.; Goto, M.; Tachino, H.; Hara, H.; Hirasawa, E.; Tagawa, H.; Muroga, Y.; Yano, S. *Macromolecules* **2000**, *33*, 9044.
(7) Agarwal, P. K.; Lundberg, R. D. *Macromolecules* **1984**, *17*, 1918.
(8) MacKnight, W. J.; Lundberg, R. D. *Rubber Chem. Technol.* **1984**, *57*, 652.
(9) Paeglis, A. U.; O'Shea, F. X. *Rubber Chem. Technol.* **1988**, *61*, 223.
(10) Oostenbrink, A. J.; Gaymans, R. J. *Polymer* **1992**, *33*, 3086.
(11) Makowski, H. S.; Lundberg, R. D.; Westerman, L.; Bock, J. *Polym. Prepr.* **1978**, *19*, 292.
(12) Lundberg, R. D.; Makowski, H. S.; Westerman, L. Chapter 5 in ref 2.
(13) Lundberg, R. D.; Makowski, H. S. Chapter 2 in ref 2.
(14) Heinen, W.; Rosenmöller, C. H.; Wenzel, C. B.; De Groot, H. J. M.; Lugtenburg, J.; van Duin, M. *Macromolecules* **1996**, *29*, 1151.
(15) Wouters, M. E. L. Ph.D. Thesis, Eindhoven University of Technology, 2000.
(16) Wouters, M. E. L.; Goossens, J. G. P.; Binsbergen, F. L. *Macromolecules* **2002**, *35*, 208.
(17) Yarusso, D. J.; Cooper, S. L. *Macromolecules* **1983**, *16*, 1871.
(18) Litvinov, V. M.; Braam, A. W. M.; van der Ploeg, M. J. *Macromolecules* **2001**, *34*, 489.
(19) Bras, W.; Derbyshire, G. E.; Ryan, A. J.; Mant, G. R.; Felton, A.; Lewis, R. A.; Hall, C. J.; Greaves, G. N. *Nucl. Instrum. Methods Phys. Res.* **1993**, *A326*, 587.
(20) Huang, T. C.; Toraya, H.; Blanton, T. N.; Wu, Y. *J. Appl. Crystallogr.* **1993**, *26*, 180.
(21) Russell, T. P.; Lin, J. S.; Spooner, S.; Wignall, G. D. *J. Appl. Crystallogr.* **1988**, *21*, 629.
(22) Different sample to detector distances (1.5, 3.5, and 7 m) were used for some samples. All three experimental setups resulted in the same scattering profile. The parent EPM did not show any peak in the SAXS profile. The profiles of the MAn-*g*-EPM materials all showed only one peak at a *q*-value of approximately 0.06 Å^{-1}.
(23) McBrierty, V. J.; Packer, K. J. *Nuclear Magnetic Resonance in Solid Polymers*; Cambridge University Press: Cambridge, 1993.
(24) Zhang, S.; Mehring, M. *Chem. Phys. Let.* **1989**, *160*, 644.
(25) Kenwright, A. M.; Say, B. J. *Solid State Nucl. Magn. Reson.* **1996**, *7*, 85.
(26) Litvinov, V. M. In *Organosilicon Chemistry II. From Molecules to Materials*; Auner, N., Weiss, J., Eds.; VCH: Weinhein, Germany, 1996; p 779.
(27) Cohen-Addad, J. P. *Prog. NMR Spectrosc.* **1993**, *25*, 1.
(28) Litvinov, V. M.; Barendswaard, W.; van Duin, M. *Rubber Chem. Technol.* **1998**, *71*, 105.
(29) Weber, H. M.; Kimmich, R. *Macromolecules* **1993**, *26*, 2597.
(30) Kulagina, T. P.; Litvinov, V. M.; Summanen, K. T. *J. Polym. Sci., Part B: Polym. Phys.* **1993**, *31*, 241.
(31) Kimmich, R, Köpf, M.; Callaghan, P. *J. Polym. Sci., Part B: Polym. Phys.* **1991**, *29*, 1029.
(32) Dutta, N. K.; Choudhury, N. R.; Haidar, B.; Vidal, A.; Donnet, J. B.; Delmotte, L.; Chezau, J. M. *Polymer* **1994**, *35*, 4293.
(33) McBrierty, V. J.; Kenny, J. C. *Kautsch. Gummi Kunstst.* **1994**, *47*, 342.
(34) Litvinov, V. M.; Steeman, P. A. M. *Macromolecules* **1999**, *32*, 8476.
(35) If the network would not contain any imperfections, the gel content should be approximately 0.5−1 wt % larger than the value of (%T_2^s + %T_2^{in}), since Zn^{2+} ions are not counted for in the NMR parameter.
(36) Clauss, J.; Schmidt-Rohr, K.; Spiess, H. W. *Acta Polym.* **1993**, *22*, 1.
(37) Demco, D. E.; Johansson, A.; Tegenfeldt, J. *Solid State Nucl. Magn. Reson.* **1995**, *4*, 13.
(38) Mellinger, F.; Wilhelm, M.; Spiess, H. W. *Macromolecules* **1999**, *32*, 4686.
(39) Buda, A.; Demco, D. E.; Blümich, B. Unpublished results.
(40) Gotlib, Y. Y.; Lofshits, M. I.; Shevelev, V. A.; Lishanski, I. A.; Balanina, I. V. *Polym. Sci. USSR* **1976**, *18*, 2630.
(41) Fry, C. G.; Lind, A. C. *Macromolecules* **1988**, *21*, 1292.
(42) Simon, G.; Baumann, K.; Gronski, W. *Macromolecules* **1992**, *25*, 3624.
(43) Richter, D.; Farafo, B.; Butera, R.; Fetters, L. J.; Huand, J. S.; Ewen, B. *Macromolecules* **1993**, *26*, 795.
(44) Litvinov, V. M.; Dias, A. A. *Macromolecules* **2001**, *34*, 4051.
(45) Mark, J. E. *Rubber Chem. Technol.* **1975**, *48*, 495.
(46) De Candia, F.; Dontsov, A.; Micera, G.; Pusino, A. *Polymer* **1973**, *14*, 497.
(47) Ward, T. C.; Tobolsky, A. V. *J. Appl. Polym. Sci.* **1967**, *11*, 2903.
(48) Sakamoto, K.; MacKnight, W. J.; Porter, R. S. *J. Polym. Sci., Polym. Phys. Ed.* **1970**, *8*, 277.
(49) Eisenberg, A., Bailey, F., Eds. *Coulombic Interaction in Macromolecular Systems*; ACS Symposium Series 302; American Chemical Society: Washington, DC, 1986.
(50) Eisenberg, A. *Macromolecules* **1970**, *3*, 147.
(51) Forsmann, W. C. *Macromolecules* **1982**, *5*, 1032.
(52) Dreyfus, B. *Macromolecules* **1985**, *18*, 284.

MA020358A